SAND2015-0829C

Effects of spanwise blade load distribution on wind turbine wake evolution *

Xiaolei Yang, † Aaron Boomsma ‡ and Fotis Sotiropoulos§

Saint Anthony Falls Laboratory, Department of Civil Engineering, University of Minnesota

2 Third Avenue SE, Minneapolis, MN 55414, USA

Brian R. Resor, ¶ David C. Maniaci ‖ and Christopher L. Kelley **

Sandia National Laboratories, Albuquerque, NM 87185 and Livermore, CA 94550, USA

In this paper, the effect of two different turbine blade designs on the wake characteristics was investigated using large-eddy simulation with actuator line model. For the two different designs, the total axial load is nearly the same but the spanwise (radial) distributions are different. The one with higher load near the blade tip is denoted as Design A; the other is Design B. From the computed results, we observed that the velocity deficit from Design B is higher than that from Design A. The intensity of turbulence kinetic energy in the far wake is also higher for Design B. The effect of blade load distribution on the wind turbine axial and tangential induction factors was also investigated.

Nomenclature

μ	Dynamic viscosity
Ω	Rotational speed of turbine rotor
ρ	Air density
τ_{aero}	Aerodynamic torque on the wind turbine
τ_{ij}	Subgrid stress tensor
ξ^i	Curvilinear coordinates
a	Axial induction factor
$a^{'}$	Tangential induction factor
C_P	Power coefficient of wind turbine
C_T	Thrust coefficient of wind turbine
f_l	Body forces from wind turbine model
L_x	Computational domain size in windwise direction
L_y	Computational domain size in crosswind (y) direction
L_z	Computational domain size in crosswind (z) direction
N_x	Number of grid nodes in windwise direction
N_y	Number of grid nodes in crosswind (y) direction
N_z	Number of grid nodes in crosswind (z) direction
U^i	Contravariant volume flux in curvilinear coordinates
u_i	Velocity components in Cartesian coordinates

*Sandia National Laboratories is a multi-program laboratory managed and operated by Sandia Corporation, a wholly owned subsidiary of Lockheed Martin Corporation, for the U.S. Department of Energys National Nuclear Security Administration under contract DE-AC04-94AL85000.

†Research associate

‡Graduate student

§Professor

¶Senior Member of the Technical Staff, AIAA Member

‖Senior Member of the Technical Staff, AIAA Member

**Postdoctoral Appointee, AIAA Member

x_i	Cartesian coordinates
D	Rotor diameter
J	Jacobian of the geometric transformation
P	Power output of wind turbine
p	pressure
R	Rotor radius
T	Thrust force on wind turbine
U	Incoming wind speed

I. Introduction

TURBINE wake interaction affects wind turbine performance and lifetime. It is usually assumed that the wind speed deficit and turbulence intensity in the turbine wake primarily depend on the thrust coefficient C_T. The hypothesis in this paper is that the distribution of spanwise (radial) loading may also affect the wake behavior. This hypothesis is tested on two conceptual rotor designs, which are potential turbine candidates for the SWiFT (Scaled Wind Farm Technology) site[1,2] located at the Reese Technology Center near Lubbock, TX, USA.

The effect of the different load distributions on turbine wake is investigated using the Virtual Wind Simulator (VWiS) developed at Saint Anthony Falls Laboratory, University of Minnesota. In VWiS, the wind field is simulated using large-eddy simulation. The turbine blades are modelled as an actuator disk or actuator lines. The actuator disk LES model of VWiS was applied to simulate infinite turbine arrays.[3] The actuator line LES model of VWiS was validated using wind tunnel and field measurements and applied to a site with complex terrain.[4] The actuator line LES model was also applied to simulate turbulent flow past an axial flow hydrokinetic turbine placed in an open channel flow[5] with reasonable agreement with the measurement.[6]

II. Numerical methods: the VWiS code

The governing equations are the three-dimensional, unsteady, filtered continuity and Navier-Stokes equations. The Virtual Wind Simulator (VWiS) computer code, introduced and validated with wind tunnel and field measurements by Yang et al.,[4] is used to solve these equations. The code employs the curvilinear immersed boundary (CURVIB) method,[7] which enables simulations of turbines placed in arbitrarily complex terrain.[4] The governing equations are first written in Cartesian coordinates x_i and then transformed fully (both the velocity vector and spatial coordinates) in non-orthogonal, generalized, curvilinear coordinates ξ^i. The transformed equations read in compact tensor notation (repeated indices imply summation) as follows $(i, j = 1, 2, 3)$:

$$J\frac{\partial U^i}{\partial \xi^i} = 0, \tag{1}$$

$$\frac{1}{J}\frac{\partial U^i}{\partial t} = \frac{\xi_l^i}{J}\left(-\frac{\partial}{\partial \xi^j}(U^j u_l) + \frac{\mu}{\rho}\frac{\partial}{\partial \xi^j}\left(\frac{g^{jk}}{J}\frac{\partial u_l}{\partial \xi^k}\right) - \frac{1}{\rho}\frac{\partial}{\partial \xi^j}\left(\frac{\xi_l^j p}{J}\right) - \frac{1}{\rho}\frac{\partial \tau_{lj}}{\partial \xi^j} + f_l\right), \tag{2}$$

where $\xi_l^i = \partial \xi^i / \partial x_l$ are the transformation metrics, J is the Jacobian of the geometric transformation, u_i is the i^{th} component of the velocity vector in Cartesian coordinates, $U^i = (\xi_m^i / J) u_m$ is the contravariant volume flux, $g^{jk} = \xi_l^j \xi_l^k$ are the components of the contravariant metric tensor, ρ is the density, μ is the dynamic viscosity, p is the pressure, $f_l (l = 1, 2, 3)$ are the body forces introduced by the wind turbines and τ_{ij} represents the anisotropic part of the subgrid scale stress tensor, which is modelled by the dynamic eddy-viscosity subgrid scale model.[8]

The actuator line model proposed by Sorensen and Shen,[9] is employed for parameterizing the wind turbine blades. In the actuator line model, the blade of a wind turbine rotor is modelled by a straight rotating line. Forces are distributed on each line (blade) to represent the effects of wind on the blades. The forces are calculated based on a blade element approach, which divides the blade into discrete elements in the radial direction and employs tabulated airfoil data (chord, twist, drag and lift coefficients) and the instantaneous, local wind velocity to calculate the local force acting on each blade element. The forces on the blades are distributed from the actuator line to the surrounding background grid nodes using the smoothed discrete

delta function proposed in.[10] The advantage of using a discrete delta function for force distribution is that the forces are distributed only on the surrounding grid cells (usually two to five depending on the selected discrete delta function) with conservation of the total force and torque.

III. Results

Two different designs with the same turbine thrust coefficient C_T are considered: the first with higher load near the blade tip is denoted as Design A; the second is Design B. The different distributions of the forces over the blade for Design A and Design B are achieved using different radial distributions of the chord length and the local pitch angle of the blade, which are shown in figure 1 (a) and (b), respectively. As seen the chord length from Design B is significantly smaller than Design A near the tip, while larger than Design A for inboard locations within about $0.2 < r/R < 0.85$. The local pitch angle from Design B, on the other hand, is higher than Design A for the near tip region (about $r/R > 0.85$), while lower than Design A for all the other region.

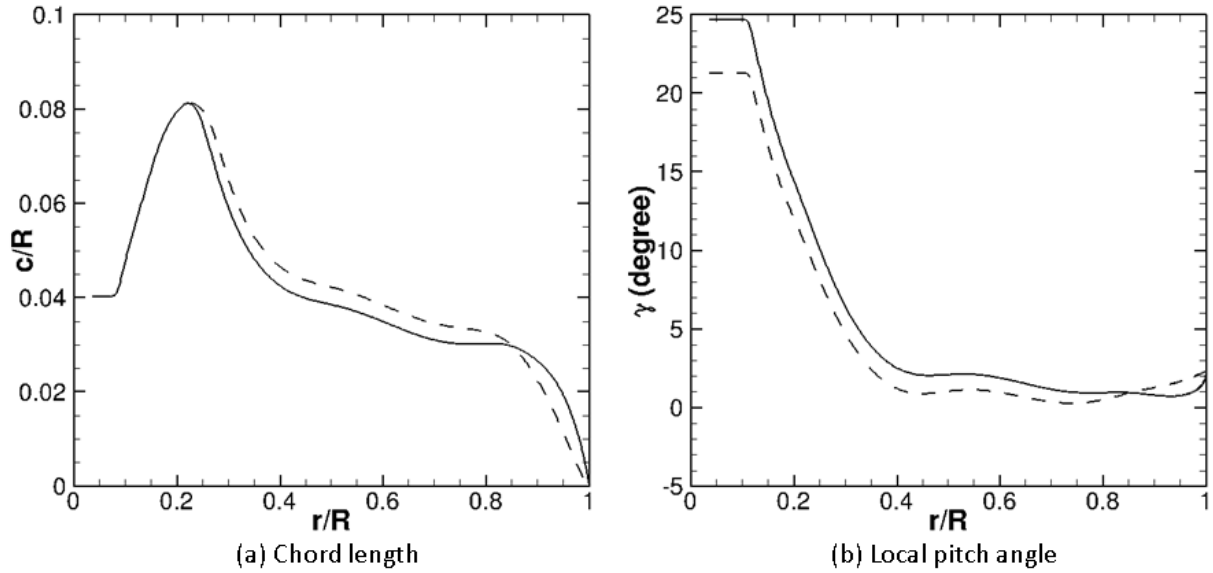

Figure 1. Radial distributions of the chord length (a) and local pitch angle (b) on the blade. Solid lines: Design A; dashed lines: Design B.

LES are carried out both for Design A and Design B. The Reynolds number based on the incoming wind speed U and the rotor diameter D, which is 27 meters, is 1.5×10^7. The tip speed ratio is 9. The size of the computational domain is $L_x \times L_y \times L_z = 18D \times 8D \times 8D$, in which x represents the wind direction, and y and z represent the crosswind directions, respectively. The total grid number is $N_x \times N_y \times N_z = 1531 \times 461 \times 461$. The meshes were uniform near the turbine with grid spacing $D/200$ in all directions. Uniform wind is fed at the inlet. Neumann boundary condition is applied at the outlet. Free-slip boundary condition was applied at the crosswind boundaries. The time step is $4 \times 10^{-4} U/D$. The simulations were carried out until the total kinetic energy achieved statistically steady state. The time-averaged flow fields were obtained by averaging for about 50 turbine revolution periods.

The computed mean power coefficient C_P, which is calculated as follows:

$$C_P = \frac{P}{0.5\rho\pi R^2 U^3}, \tag{3}$$

where the power $P = \tau_{aero}\Omega$ (in which τ_{aero} is the aerodynamics torque on the turbine blades and Ω is the rotational speed of the rotor, respectively), is 0.514 and 0.492 for Designs A and B, respectively. The higher C_P for Design A is consistent with the design philosophy that Design A is a power optimized design. The

mean thrust coefficient, defined as

$$C_T = \frac{T}{0.5\rho\pi R^2 U^2}, \tag{4}$$

where T is the thrust force on the turbine, is also calculated for Design A and Design B. The computed C_T is 0.635 and 0.628 for Design A and Design B, respectively. That is, both designs have essentially the same thrust coefficient.

The distributions of the axial and tangential loads on the blade are compared in figure 2. As seen both axial and tangential loads from Design B are smaller than Design A for the near tip region (about $r/R > 0.75$), while larger than Design A for inboard region for about $0.25 < r/R < 0.75$.

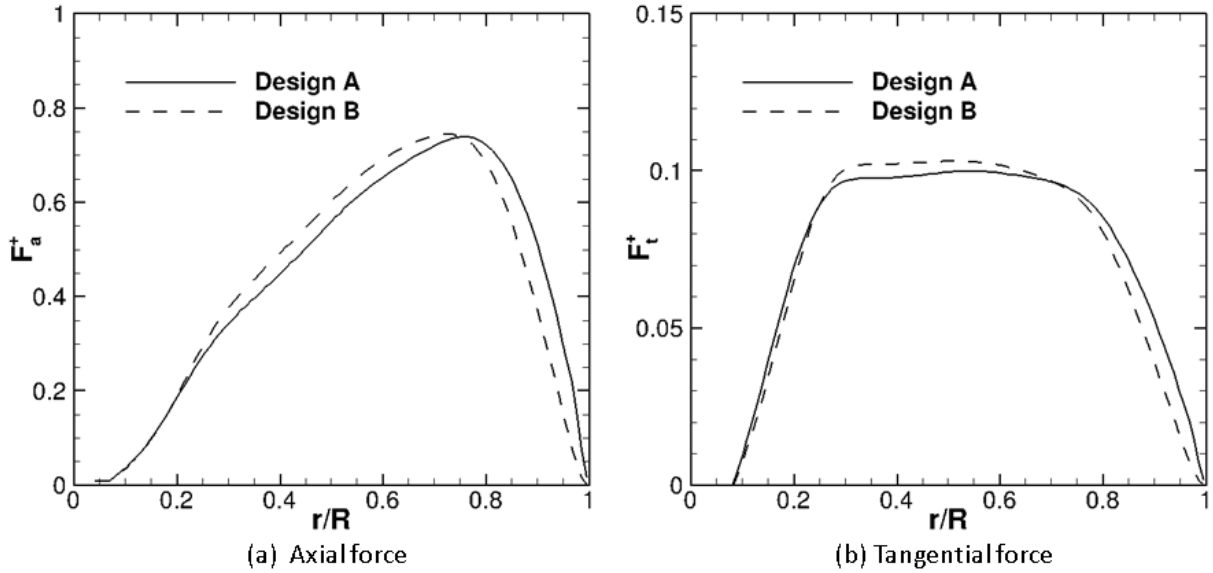

Figure 2. Distributions of the axial (a) and tangential (b) loads along the blade, which are normalized by $\frac{1}{2}\rho\pi R^2U^2$ (where R is the rotor radius).

The time-averaged flow fields from Design A and Design B are shown in figures 3, 4 and 5 for the contours of windwise velocity, rotational velocity and turbulence kinetic energy (TKE), respectively. As seen, the velocity deficit for Design B is larger than Design A until far downwind (about 12D) in the turbine wake. The rotational components, on the other hand, persist longer in the wake for Design A. The intensity of the TKE generated from the rotor tip shear layer is nearly the same for Design A and Design B from 4D to 7D turbine downwind. From 7D to further downwind locations, however, the TKE for design B starts increasing significantly and is distributed in a more wider region and with a much higher intensity than Design A. This finding may suggest different far-wake meandering and/or instability patterns for the two turbine designs.

The radial profiles of the time and azimuthal-averaged windwise velocity are plotted in figure 6 for the turbine near wake region. In the inboard wake region, it is observed that the velocity deficit for Design B is larger than Design A at $x = 0.5D$ for $0.2 < r/R < 0.9$, which becomes wider for further downwind locations. In the near tip region, on the other hand, a higher velocity deficit for Design A is observed. The above observations are consistent with the load distribution shown in figure 2. However, the larger velocity deficit for Design A is distributed in a very narrow region and disappear rapidly from 0.5D to 3D turbine downwind locations.

The axial and tangential induction factors defined as follows

$$a = 1 - \frac{\langle u \rangle}{U}, \tag{5}$$

and

$$a^{'} = -\frac{\langle u_\theta \rangle}{\Omega r}, \tag{6}$$

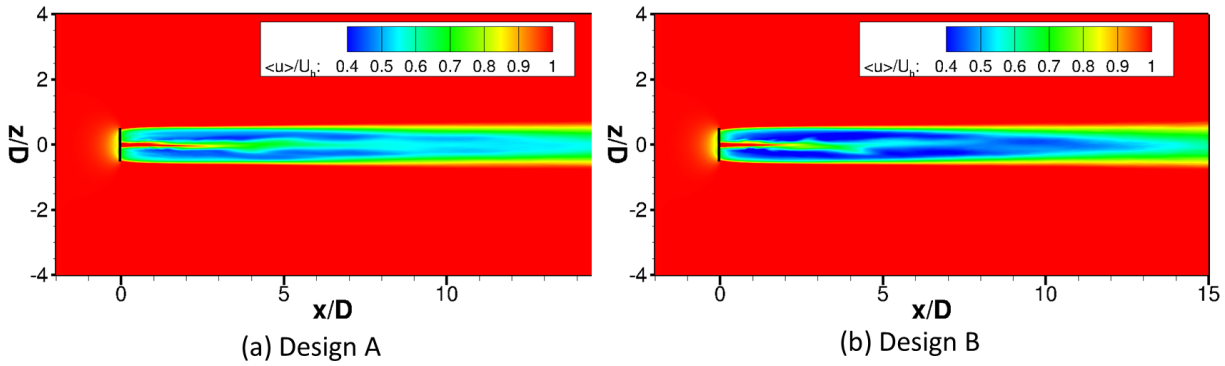

Figure 3. Comparison of the time-averaged windwise velocity contours between Design A and Design B.

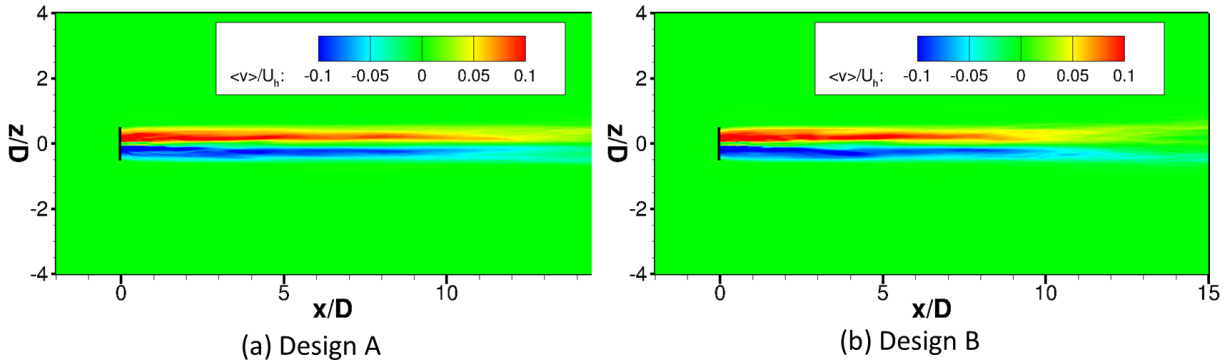

Figure 4. Comparison of the time-averaged rotational velocity contours between Design A and Design B.

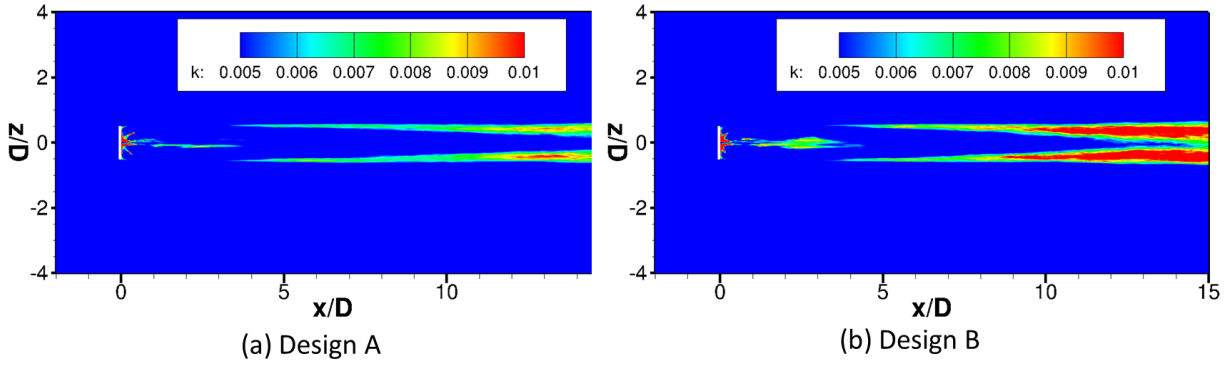

Figure 5. Comparison of the turbulence kinetic energy contours between Design A and Design B.

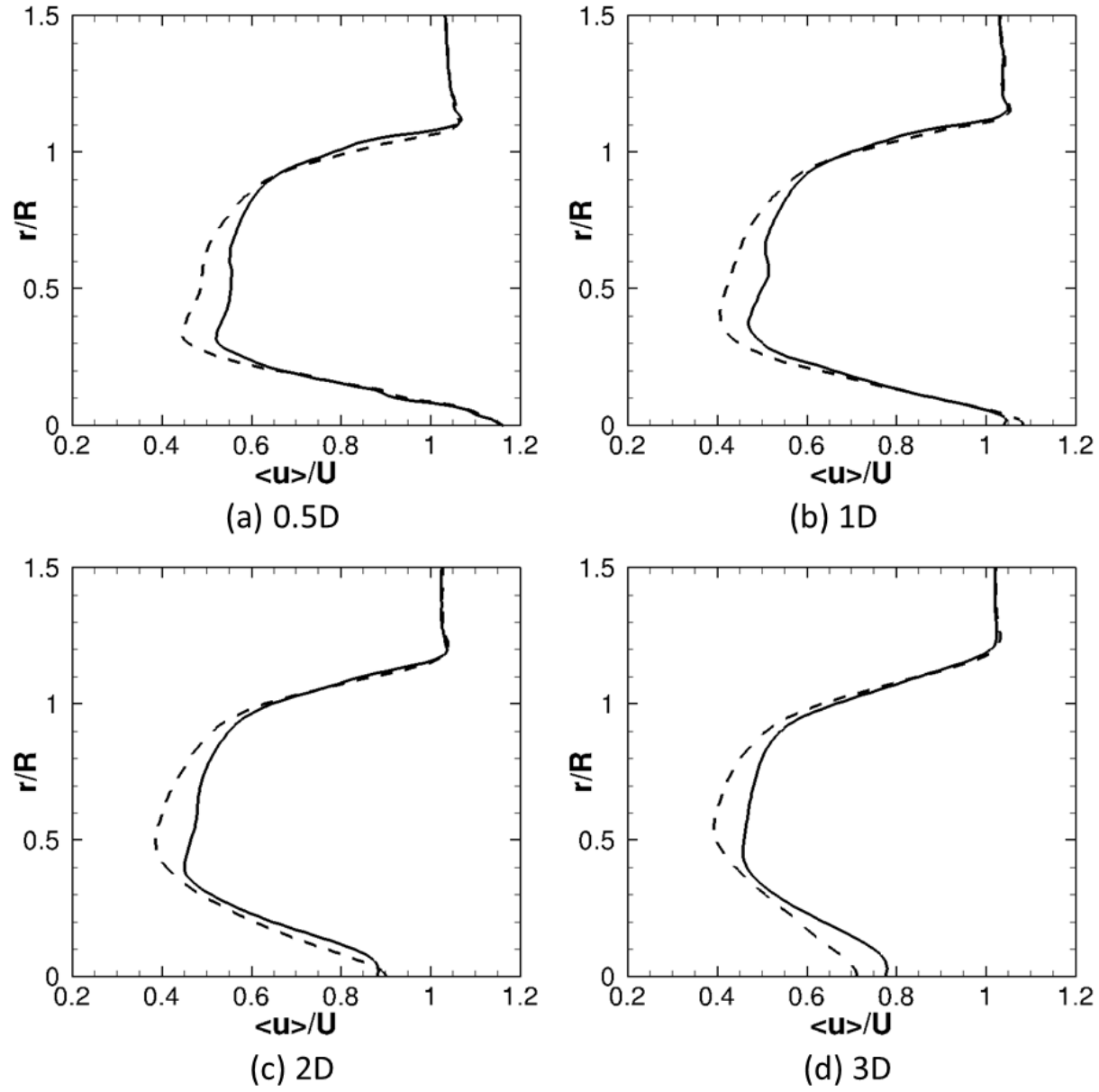

Figure 6. Radial profiles of the time and azimuthal-averaged windwise velocity at different downwind directions. Solid lines: design A; dashed lines: design B.

where u_θ is the azimuthal velocity on the rotor plan, are plotted in figure 7. As shown in figure 7 (a), the axial induction factor for Design B is larger for $0.2 < r/R < 0.8$, while smaller for $r/R > 0.8$ in comparison with Design A. For the tangential induction factor, however, the difference between the two different designs are very small. The mean axial induction factor, which is calculated by averaging the axial induction factor

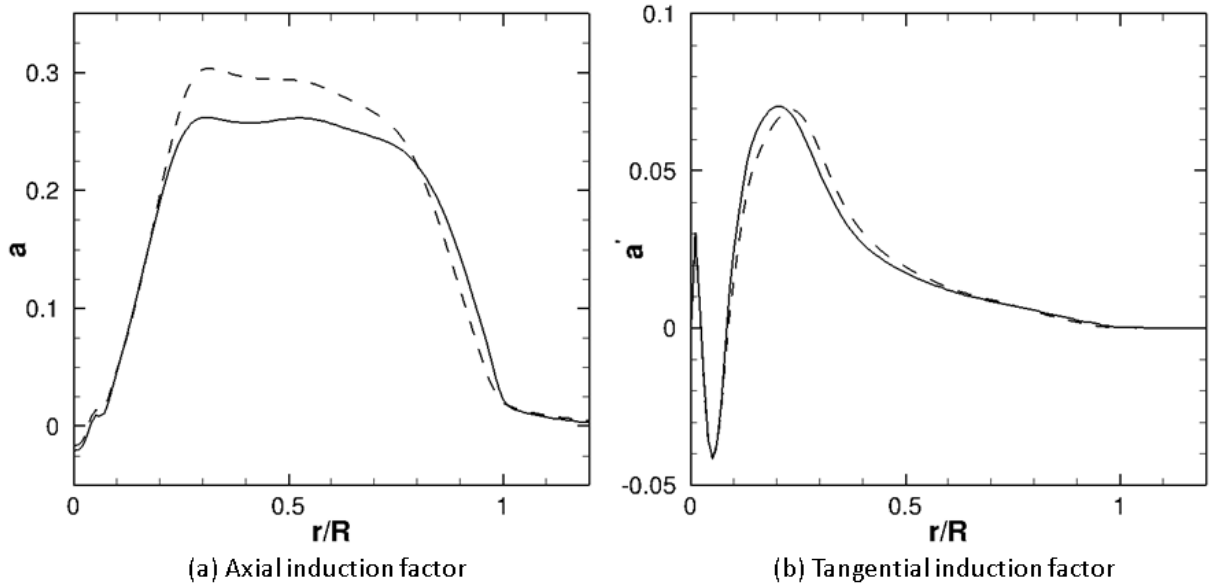

Figure 7. Radial profiles of the axial and tangential induction factors. Solid lines: design A; dashed lines: design B.

(figure 7 (a)) from 0 to R, is 0.190 and 0.203 for Design A and Design B, respectively. It is thus noted that the relative difference between the two mean induction factors are considerably small, i.e. around 7% of the mean. However, the local difference in the windwise velocity can be as high as 20% difference between the two designs and can persist into very far turbine wake as seen in figures 3 and 6. This observation implies that wind turbine models assuming uniform force distribution will not be able to capture the effect of force distribution on turbine wake even though the mean axial forces are the same. The mean axial induction factor can also be calculated from the mean axial load by employing the one-dimensional momentum theory, in which the relation between C_T and the axial induction factor is

$$C_T = 4a(1-a). \tag{7}$$

The mean axial induction factor calculated from the above relation is 0.151 and 0.143 for Design A and Design B, respectively. This inconsistency is possibly because the rotational effect is not taken into account in deriving the above equation, which is significant when the tip-speed ratio is high.

IV. Summary

Two simulations on Design A and Design B have been carried out, for which the mean axial loads are nearly same but the distributions are different. In comparison with Design A, the loads are higher in the inboard region, while smaller in the near tip region for Design B. From the computed results, considerable differences on the windwise velocity, rotational velocity, turbulent kinetic energy in the turbine wake are observed for the two different designs. The Design B produces higher velocity deficit until the very far (about 12D) turbine wake region. In the very far wake region, where transition to turbulence occur, the intensity of turbulent kinetic energy from Design B is also significantly higher. It is observed that the axial induction factor is higher in the inboard region for Design B. The differences in the tangential induction factor, on the other hand, are not very significant. It is also observed that the mean axial induction factor calculated based on one-dimensional theory is not the same as the one computed from LES with actuator line model. This is probably because the former approach does not take into account the rotational effect. Simulations of the turbine wake under turbulent inflow will be carried out in future work.

Acknowledgement

This work was supported by Department of Energy DOE (DE-EE0002980, DE-EE0005482 and DE-AC04-94AL85000). Computational resources were provided by Sandia National Laboratories and the University of Minnesota Supercomputing Institute.

References

[1]Barone, M. and White, J., "DOE/SNL–TTU Scaled Wind Farm Technology Facility: Research Opportunities for Study of Turbine-Turbine Interaction," *SANDIA REPORT, SAND2011-6522*, 2011.

[2]Berg, J., Bryant, J., LeBlanc, B., Maniaci, D., Naughton, B., Paquette, J., Resor, B., White, J., and Kroeker, D., "Scaled Wind Farm Technology Facility Overview," *AIAA SciTech, 13-17 January 2014, National Harbor, Maryland, 32nd ASME Wind Energy Symposium, AIAA 2014-1088*, 2014.

[3]Yang, X., Kang, S., and Sotiropoulos, F., "Computational study and modeling of turbine spacing effects in infinite aligned wind farms," *Physics of Fluids*, Vol. 24, No. 11, 2012, pp. 115107.

[4]Yang, X., Sotiropoulos, F., Conzemius, R. J., Wachtler, J. N., and Strong, M. B., "Large-eddy simulation of turbulent flow past wind turbines/farms: the Virtual Wind Simulator (VWiS)," *Wind Energy*, 2014.

[5]Kang, S., Yang, X., and Sotiropoulos, F., "On the onset of wake meandering for an axial flow turbine in a turbulent open channel flow," *Journal of Fluid Mechanics*, Vol. 744, 2014, pp. 376–403.

[6]Chamorro, L., Hill, C., Morton, S., Ellis, C., Arndt, R., and Sotiropoulos, F., "On the interaction between a turbulent open channel flow and an axial-flow turbine," *Journal of Fluid Mechanics*, Vol. 716, 2013, pp. 658–670.

[7]Ge, L. and Sotiropoulos, F., "A numerical method for solving the 3D unsteady incompressible Navier-Stokes equations in curvilinear domains with complex immersed boundaries," *J. Comput. Phys.*, Vol. 225, No. 2, 2007, pp. 1782–1809.

[8]Germano, M., Piomelli, U., Moin, P., and Cabot, W. H., "A dynamic subgrid-scale eddy viscosity model," *Phys. Fluids A*, Vol. 3, No. 7, 1991, pp. 1760–1765.

[9]Sørensen, J. N. and Shen, W. Z., "Numerical modeling of wind turbine wakes," *J. Fluid Eng. Trans. ASME*, Vol. 124, 2002, pp. 393–399.

[10]Yang, X., Zhang, X., Li, Z., and He, G.-W., "A smoothing technique for discrete delta functions with application to immersed boundary method in moving boundary simulations," *J. Comput. Phys.*, Vol. 228, 2009, pp. 7821–7836.